引用格式：KANG Xinwei, DAI Pengpeng. Preparation and Luminescence Properties of Color-tunable Emission $Cs_3Gd_{1-x-y}Lu_yGe_3O_9:xBi^{3+}$ Solid Solution Phosphor[J]. Acta Photonica Sinica, 2022, 51(12):1216002
康新威,戴鹏鹏. 发光颜色可调 $Cs_3Gd_{1-x-y}Lu_yGe_3O_9:xBi^{3+}$ 固溶体荧光粉的制备和发光性质研究[J]. 光子学报,2022,51(12):1216002

发光颜色可调 $Cs_3Gd_{1-x-y}Lu_yGe_3O_9:xBi^{3+}$ 固溶体荧光粉的制备和发光性质研究

康新威,戴鹏鹏
(新疆师范大学 物理与电子工程学院 新疆发光矿物与光功能材料研究重点实验室,乌鲁木齐 830054)

摘　要：采用传统的高温固相法合成了一系列 $Cs_3Gd_{1-x}Ge_3O_9:xBi^{3+}$(0.02≤$x$≤0.1)蓝色荧光粉,并通过 Lu^{3+} 替代 $Cs_3Gd_{1-x}Ge_3O_9$ 基质中的 Gd^{3+},调控激活剂 Bi^{3+} 周围局部环境,制备了一系列发光颜色可调的 $Cs_3Gd_{0.96-y}Lu_yGe_3O_9:0.04Bi^{3+}$(0.1≤$y$≤0.9)固溶体荧光粉。X射线衍射、稳态/瞬态荧光光谱、变温光谱对荧光粉样品的物相结构、发光特性、荧光寿命、热稳定性进行了详细表征。结果表明,我们成功合成了一系列纯相的 $Cs_3Gd_{1-x-y}Lu_yGe_3O_9:xBi^{3+}$ 化合物。在紫外光 330 nm 激发下,$Cs_3Gd_{1-x}Ge_3O_9:xBi^{3+}$ 荧光粉的发射峰位于 452 nm,呈现蓝光发射,该宽带发射峰源于 Bi^{3+} 的 $^3P_1\rightarrow{}^1S_0$ 跃迁,Bi^{3+} 掺杂浓度为 0.04 mol 时,$Cs_3Gd_{1-x}Ge_3O_9:xBi^{3+}$ 荧光粉的荧光强度达到最大值。在最优 Bi^{3+} 掺杂浓度下,通过 Lu^{3+} 替代基质中的 Gd^{3+},发现合成的一系列 $Cs_3Gd_{0.96-y}Lu_yGe_3O_9:0.04Bi^{3+}$(0.1≤$y$≤0.9)固溶体荧光粉发射峰逐渐发生红移,随着 Lu^{3+} 掺杂浓度的逐渐增加,发射峰从 x=0.1 mol 时的 453 nm 逐渐红移至 x=0.9 mol 时的 483 nm,相应的半峰宽从 88 nm 展宽至 116 nm,色坐标从蓝色区域(0.168 5,0.160 2)过渡到青色区域(0.217 9,0.300 7)。样品光谱行为的变化主要是因为晶体场劈裂程度增大和斯托斯克位移增大。探究了 x=0.04 mol、y=0.5 mol 样品的发光热稳定性,当温度升高到 423 K 时样品的发光强度保持在初始值的 55%。所得到的一系列发光颜色可调的固溶体荧光粉在全光谱照明、植物照明等领域具有潜在的应用。

关键词：颜色可调;固溶体;Bi^{3+} 掺杂;宽带发射;全光谱
中图分类号：O482.31　　**文献标识码**：A　　**doi**：10.3788/gzxb20225112.1216002

0　引言

荧光粉转换白光发光二极管(pc-WLED)具有长寿命、环保、低能耗和高亮度等优点,已广泛应用于照明领域[1-3]。目前商用白光 LED 是采用蓝色芯片组合 $Y_3Al_5O_{12}:Ce^{3+}$ 黄色荧光粉而成,然而该方式产生的白光 LED 由于发射光谱中缺少红色成份,导致其显色指数较低(CRI<75),相关色温较高(CCT>4 500K),无法满足室内照明需求[4-7]。国内外研究者们提出了一种改进的方式,通过近紫外芯片激发三基色(红、绿、蓝)荧光粉来获得白光 LED,该方法虽然可以产生室内照明所需的暖白光,但是在可见光光谱中的青色区域(480~520 nm)存在一个明显的“青色间隙”,使实现全光谱照明具有挑战性[8-10]。因此,人们希望获得一种青色发光材料,通过荧光粉混合的方式来实现全光谱照明。所以开发出能够被近紫外芯片驱动的青色荧光粉极为重要。

众所周知,稀土 Eu^{2+} 和 Ce^{3+} 由于其 5d~4f 允许跃迁所引起的大的吸收截面和较高的荧光量子产率,已被广泛作为激活剂离子用于无机荧光粉中[11-13]。然而,Eu^{2+}/Ce^{3+} 激活的荧光粉在可见光区域存在光谱重

基金项目：国家自然科学基金(No.51762040),新疆维吾尔自治区杰出青年科学基金 (No.2021D01E19),新疆师范大学矿物发光与微结构重点实验室研究基金(No.KWFG202208)
第一作者：康新威(1995—),男,硕士研究生,主要研究方向为固体发光。Email: 1176390344@qq.com
导师(通讯作者)：戴鹏鹏(1982—),男,教授,博士,主要研究方向为固体发光。Email: daipp614@nenu.edu.cn
收稿日期：2022-06-29;**录用日期**：2022-08-15

叠，使合成的荧光粉出现重吸收现象，最终导致合成的器件出现发光效率低、色漂移等问题[14-15]。与稀土Eu^{2+}/Ce^{3+}相比，非稀土Bi^{3+}的发光主要源于$^1S_0\sim{}^3P_1/^1P_1$跃迁，Bi^{3+}在可见光区域几乎没有吸收，所以Bi^{3+}激活的荧光粉可以有效避免稀土Eu^{2+}/Ce^{3+}遇到的光谱重吸收问题[16-17]。此外，Bi^{3+}最外层电子6s和6p裸露在外，对晶体场环境变化较为敏感，所以Bi^{3+}的发光易受到晶体场环境变化的影响而呈现出从紫外到红光的发射[18-20]。因此，Bi^{3+}被认为是一种可以实现荧光粉发光颜色调控的激活剂离子。2019年，由MORRISON G团队报道的$Cs_3REGe_3O_9$碱稀土锗酸盐引起了人们广泛关注。该结构属于正交晶系，空间群为Pna21，结构中存在两种阳离子格位，Cs^{3+}离子游离在结构的空隙之中，而其中的RE格位（RE=Pr，Nd和Sm－Yb）几乎包含了所有稀土元素。因此，该类型结构的化合物具有较强的结构灵活性和丰富的晶体场环境。最近，得益于该晶体结构的灵活性和特殊性（链状结构的横向振动），Eu^{3+}掺杂的$Cs_3GdGe_3O_9$红色荧光粉被报道，该荧光粉表现出了不同寻常的无浓度猝灭特性和负热膨胀性能[21-22]。目前关于Bi^{3+}掺杂$Cs_3GdGe_3O_9$荧光粉鲜有报道，本文采用高温固相法合成了一系列$Cs_3Gd_{1-x}Ge_3O_9:xBi^{3+}$（$0.01\leqslant x\leqslant 0.09$）蓝色荧光粉，通过等价阳离子替代策略，用$Lu^{3+}$替代$Gd^{3+}$获得了一系列发光颜色可调的$Cs_3Gd_{0.96-y}Lu_yGe_3O_9:0.04Bi^{3+}$（$0.1\leqslant y\leqslant 0.9$）固溶体荧光粉，并采用X射线衍射、稳态/瞬态荧光光谱进行表征。此外，还探究了固溶体荧光粉（$x=0.04$，$y=0$）的发光热稳定性。本文合成的一系列固溶体荧光粉在全光谱照明、植物照明等领域具有潜在的应用价值。

1 实验

1.1 样品制备

采用高温固相反应合成一系列$Cs_3(Gd_{1-x-y}Lu_y)Ge_3O_9:xBi^{3+}$（$0.02\leqslant x\leqslant 0.1$，$0.1\leqslant y\leqslant 0.9$）荧光粉。按照化学计量比精确称量，原料为$Cs_2CO_3$（99.9%）、$Gd_2O_3$（99.99%）、$Lu_2O_3$（99.99%）、$GeO_2$（99.99%）、$Bi_2O_3$（99.99%）。将原材料混合放入研钵中，均匀研磨40 min，研磨好的粉末转移至氧化铝坩埚，放入马弗炉中加热至1 000 ℃，在空气气氛下，煅烧8 h。反应停止后，待马弗炉自然冷却至室温后取出，将退火后的样品再次研磨，得到最终的粉末样品。

1.2 样品表征

使用日本岛津XRD-700型粉末衍射仪收集样品的X射线衍射（X Ray Diffraction，XRD）数据。Cu-Kα1射线为射线源，工作电压和工作电流分别为40 kV和30 mA，扫描范围2θ为20°～50°，扫描速度固定在5(°)/min。样品的漫反射光谱使用紫外-可见漫反射光谱仪（UV-2550 PC，日本岛津公司）测试。样品的激发光谱、发射光谱、荧光寿命衰减曲线和变温光谱采用英国爱丁堡稳态/瞬态荧光光谱仪（FLS920）和富士电气PXF4变温附件。

2 结果与讨论

2.1 $Cs_3GdGe_3O_9$结构分析

图1(a)为$Cs_3GdGe_3O_9$晶体结构图[22]。$Cs_3GdGe_3O_9$属于正交晶系，空间群属于Pna21。GeO_4四面体通

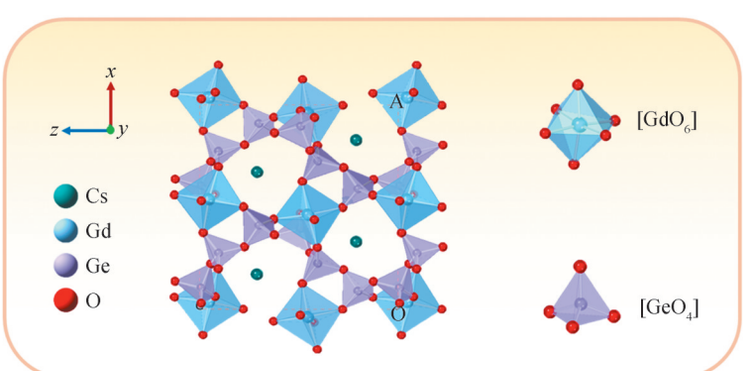

(a) Crystal structure of $Cs_3GdGe_3O_9$　　(b) Coordination environments diagram of GdO_6 and GeO_4

图1 $Cs_3GdGe_3O_9$晶体结构图和GdO_6、GeO_4的配位环境图

Fig.1 Crystal structure of $Cs_3GdGe_3O_9$ and coordination environments diagram of GdO_6 and GeO_4

过角共享形成具有Ge_6O_{18}重复单元的“之”字形链，这些“之”字形链通过GdO_6八面体连接成一个完整的框架，Cs原子占据该结构的空隙。图1(b)是GdO_6八面体和GeO_4四面体格位的配位环境，显然Gd^{3+}是由6个O原子配位形成的GdO_6八面体，Ge^{4+}是由4个O原子配位形成GeO_4四面体，多面体的存在为Bi^{3+}发光提供了良好的晶格环境。

2.2 $Cs_3Gd_{1-x}Ge_3O_9:xBi^{3+}$荧光粉的物相分析及发光性质

图2为$Cs_3Gd_{1-x}Ge_3O_9:xBi^{3+}$($0.02\leqslant x\leqslant 0.1$)(CGGO:$xBi^{3+}$)荧光粉样品的XRD图谱和XRD放大图。样品的衍射峰位与$Cs_3GdGe_3O_9$标准卡片(CCDC#1909042)一致，未出现其他杂质峰，证明成功合成了不同浓度的CGGO:xBi^{3+}($0.02\leqslant x\leqslant 0.1$)荧光粉。26.5°～27°范围内放大后的XRD图谱可看出随着Bi^{3+}浓度的增加，样品的衍射峰逐渐向小角度方向偏移，这归因于Bi^{3+}的离子半径($r=0.103$ nm，CN=6)大于Gd^{3+}的离子半径($r=0.093\,8$ nm，CN=6)，Bi^{3+}倾向于占据Gd^{3+}格位，导致晶胞扩张和晶面间距增大，衍射峰向小角度偏移，说明Bi^{3+}成功进入到CGGO基质晶格中。

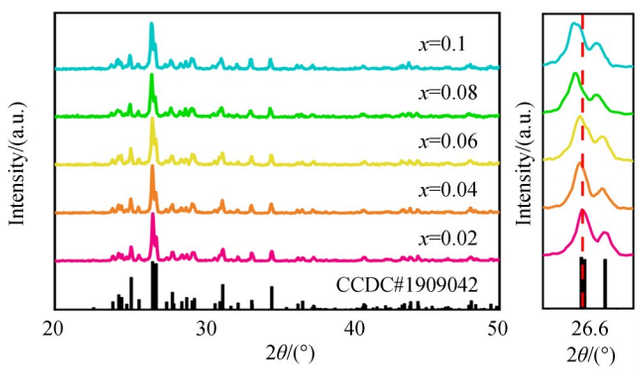

图2 CGGO:xBi^{3+}($0.02\leqslant x\leqslant 0.1$)样品的XRD图谱和放大图

Fig.2 XRD patterns and magnified XRD patterns of CGGO:xBi^{3+} ($0.02\leqslant x\leqslant 0.1$) samples

图3(a)为CGGO:$0.04Bi^{3+}$样品的归一化激发光谱与发射光谱。样品在250～360 nm处存在两处明显的激发峰，这是由于Bi^{3+}的$6s^2\rightarrow 6s6p$电子跃迁。$^1S_0-{}^3P_1$电荷跃迁发生在紫外区域，$^1S_0-{}^1P_1$电荷跃迁发生在真空紫外区域，分别对应两处激发峰。在近紫外光330 nm激发下，CGGO:$0.04Bi^{3+}$荧光粉的发射峰值位于452 nm处，发射峰不仅覆盖促进植物生长发育的450～460 nm波段，同时覆盖青色光谱缺失的480～520 nm波段，发射峰源于$^3P_1-{}^1S_0$跃迁。插图为发射强度随Bi^{3+}浓度变化关系。当Bi^{3+}掺杂浓度为0.04 mol时，样品发光强度达到最大值，荧光内量子产率为20.9%，当继续增加Bi^{3+}浓度，发射强度呈现降低趋势。这可能是由于Bi^{3+}浓度猝灭效应。荧光寿命衰减曲线能够证明上述猜想。图3(b)为样品的荧光寿命衰减曲线图谱。样品的平均寿命可通过式(1)计算[23]。

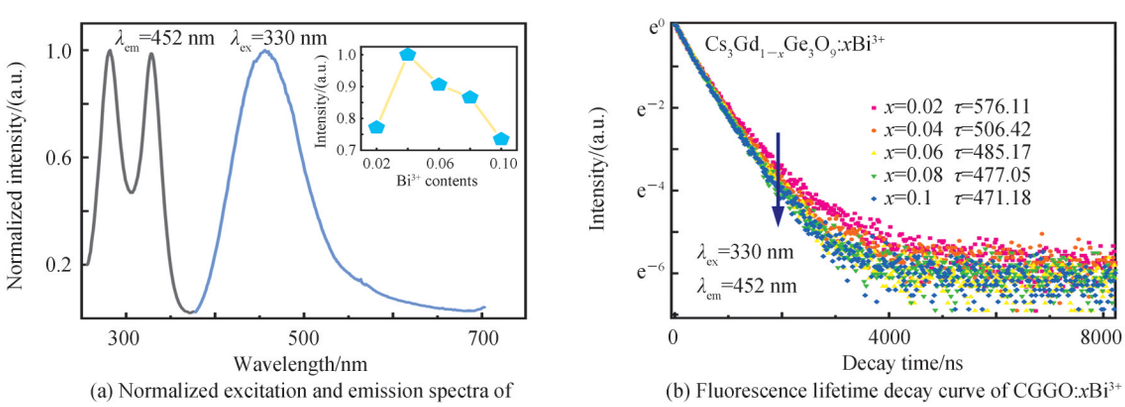

(a) Normalized excitation and emission spectra of CGGO:$0.04Bi^{3+}$

(b) Fluorescence lifetime decay curve of CGGO:xBi^{3+} ($0.02\leqslant x\leqslant 0.1$) samples

图3 CGGO:$0.04Bi^{3+}$样品的归一化激发与发射光谱和荧光寿命衰减曲线

Fig.3 Normalized excitation and emission spectra and fluorescence lifetime decay curve of CGGO:$0.04Bi^{3+}$

$$\tau=\frac{A_1\tau_1^2+A_2\tau_2^2}{A_1\tau_1+A_2\tau_2} \tag{1}$$

计算结果表明CGGO:xBi^{3+}(0.02≤x≤0.1)荧光粉的平均寿命分别是576.11、506.42、485.17、477.05、471.18 ns。当Bi^{3+}浓度增加时,相邻发光中心之间的能量传递增强,非辐射跃迁随掺杂离子浓度的增加而逐渐增强,样品的荧光寿命逐渐减小。因此,荧光寿命的衰减进一步证明了Bi^{3+}浓度猝灭的可能。

2.3 $Cs_3(Gd_{0.96-y}Lu_y)Ge_3O_9$:0.04Bi^{3+}荧光粉的物相分析

局部晶格修饰是对荧光粉发光性能改进和调控的常用手段之一。基于CGGO:0.04Bi^{3+}荧光粉,本文以Lu^{3+}替代基质中的Gd^{3+},通过调控Bi^{3+}周围局部环境,实现对发射光谱的调节。图4(a)表示$Cs_3(Gd_{0.96-y}Lu_y)Ge_3O_9$:0.04Bi^{3+}(0.1≤$y$≤0.9)(CGLGO:0.04Bi^{3+})荧光粉XRD图谱和XRD放大图。样品的衍射峰位与$Cs_3GdGe_3O_9$标准卡片(CCDC#1909042)一致,未出现其他杂质峰,证明合成的荧光粉为纯相。26.5°~27°范围内放大后的衍射峰逐渐向大角度方向偏移,这是因为Lu^{3+}离子半径(r=0.086 1 nm,CN=6)小于Gd^{3+}离子半径(r=0.093 8 nm,CN=6),Lu^{3+}的引入导致晶胞收缩和晶面间距减小。为了进一步分析Lu^{3+}的引入对晶胞的影响,图4(b)为晶胞参数变化图。随着Lu^{3+}浓度的增加,样品的晶胞参数与体积呈减小趋势,这与XRD数据相吻合。

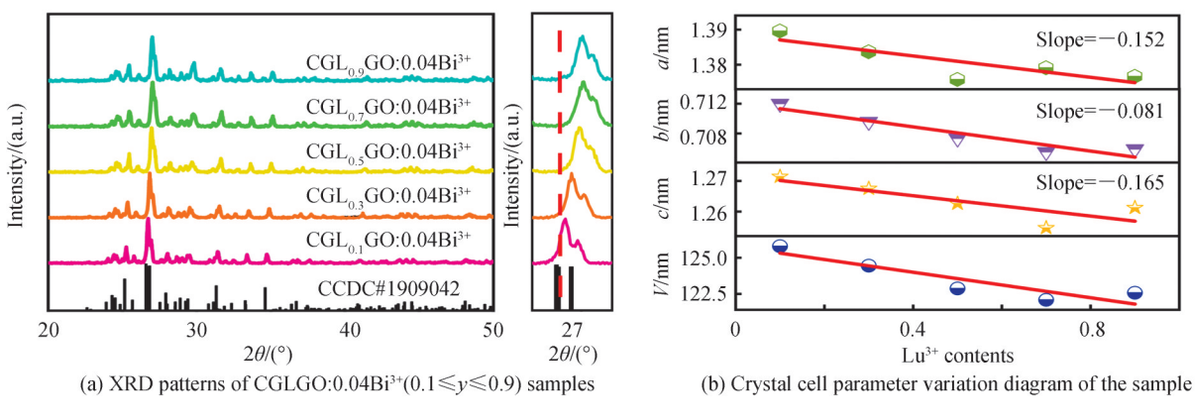

(a) XRD patterns of CGLGO:0.04Bi^{3+}(0.1≤y≤0.9) samples　(b) Crystal cell parameter variation diagram of the sample

图4 CGLGO:0.04Bi^{3+}(0.1≤y≤0.9)样品的XRD图谱和放大图以及晶胞参数变化图

Fig.4 XRD patterns and magnified XRD patterns and crystal cell parameter variation diagram of CGLGO:0.04Bi^{3+} (0.1≤y≤0.9) samples

2.4 $Cs_3(Gd_{0.96-y}Lu_y)Ge_3O_9$:0.04Bi^{3+}荧光粉的发光性质

图5(a)为荧光粉样品的漫反射光谱,表明基质材料在250~360 nm无明显吸收,CGGO:0.04Bi^{3+}和$CGL_{0.5}GO$:0.04Bi^{3+}样品在该波段具有较强的吸收,这是因为Bi^{3+}离子的$6s^2$→6s6p电子跃迁吸收。图5(b)为荧光粉样品的光学带隙。由式(2)、(3)计算CGGO:0.04Bi^{3+}和$CGL_{0.5}GO$:0.04Bi^{3+}荧光粉样品的光学带隙值[24-25]。

$$\left[F(R)h\nu\right]^n=A\left(h\nu-E_g\right) \tag{2}$$

$$F(R)=(1-R^2)/2R \tag{3}$$

式中,$h\nu$表示光子能量,A代表比例常数,E_g代表带隙值,$F(R)$代表吸收,n=1/2。CGGO:0.04Bi^{3+}与$CGL_{0.5}GO$:0.04Bi^{3+}荧光粉对应的E_g值分别为3.17 eV和3.13 eV。带隙值的变化说明Lu^{3+}进入了基质晶格中,使荧光粉的结构发生了变化,该结果与XRD数据一致。

图6(a)为CGLGO:0.04Bi^{3+}(0.1≤y≤0.9)荧光粉的归一化激发光谱。在掺杂不同Lu^{3+}浓度下,荧光粉样品的激发峰位置及峰形状基本相同,分别在278 nm和330 nm处存在明显的激发峰,这是由于Bi^{3+}从$^1S_0$基态到$^1P_1$激发态和$^3P_1$激发态的特征跃迁。同时,荧光粉样品呈现出的较宽激发带,也与漫反射光谱相对应。图6(b)为CGLGO:0.04Bi^{3+}(0.1≤y≤0.9)荧光粉归一化发射光谱。在近紫外光330 nm激发下,当y=0.1时,样品呈现蓝光发射,当y=0.9时,样品呈现宽带青光发射,Lu^{3+}的引入使发射峰逐渐发生红移,因此我们得到了适合弥补“青色间隙”的青光。插图为发射峰位随Lu^{3+}浓度变化关系。能够清晰看出荧光粉样品随Lu^{3+}浓度的增加,发射峰逐渐从453 nm红移至483 nm处。通常情况下,荧光粉发射光谱红移是由于取代离

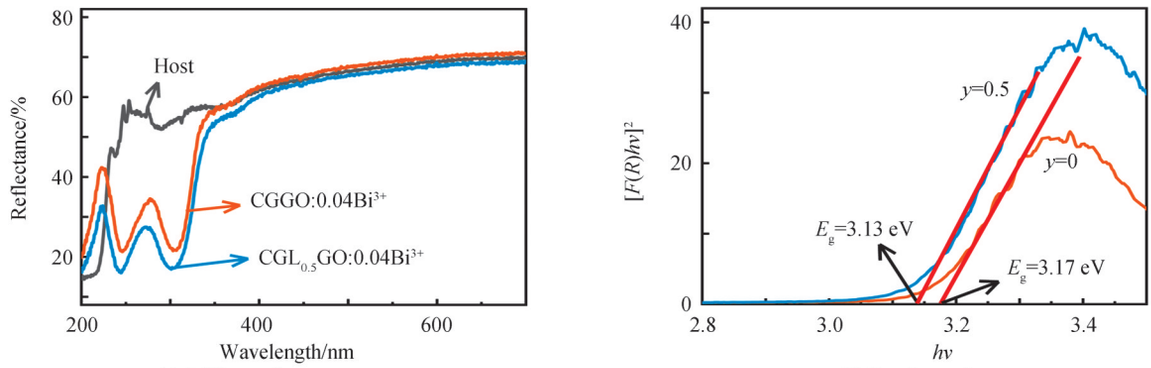

(a) Diffuse reflectance spectra　　(b) Band gap diagram

图5　CGGO，CGGO:0.04Bi^{3+}，$CGL_{0.5}GO$:0.04Bi^{3+}样品的漫反射光谱和y=0，y=0.5时样品的带隙

Fig.5　Diffuse reflectance spectra of CGGO, CGGO:0.04Bi^{3+}, $CGL_{0.5}GO$:0.04Bi^{3+} and band gap diagram of phosphor sample at y=0, y=0.5

子尺寸不匹配引起的晶体场劈裂及斯托克斯位移增大所致[26]。晶体场强度变化表示为[27]

$$D_q=\frac{1}{6}Ze^2\frac{r^4}{R^5} \tag{4}$$

式中，D_q是晶体场强度，Z是负电荷，e是电子电荷，r是d波函数的半径，R是键长。当半径较大的Gd^{3+}被半径较小的Lu^{3+}逐渐替代时，晶胞呈现收缩趋势，使得R值逐渐减小，D_q逐渐增强，从而导致Bi^{3+}晶体场劈裂程度增大，因此发射光谱向长波长移动。此外，斯托克斯位移增大也会造成发射光谱红移现象，斯托克斯位移是指发射峰主峰与激发峰主峰之间的能量差值。图6(c)为CGLGO:0.04Bi^{3+}(0.1≤y≤0.9)荧光粉斯托克斯位移及半峰宽随Lu^{3+}浓度变化的关系。随着Lu^{3+}浓度的增加，斯托克斯位移逐渐增大(9 115 cm^{-1}，9 159 cm^{-1}，9 433 cm^{-1}，9 541 cm^{-1}，9 984 cm^{-1})，半峰宽受斯托克斯位移影响也逐渐展宽，从88 nm展宽至116 nm。因此，

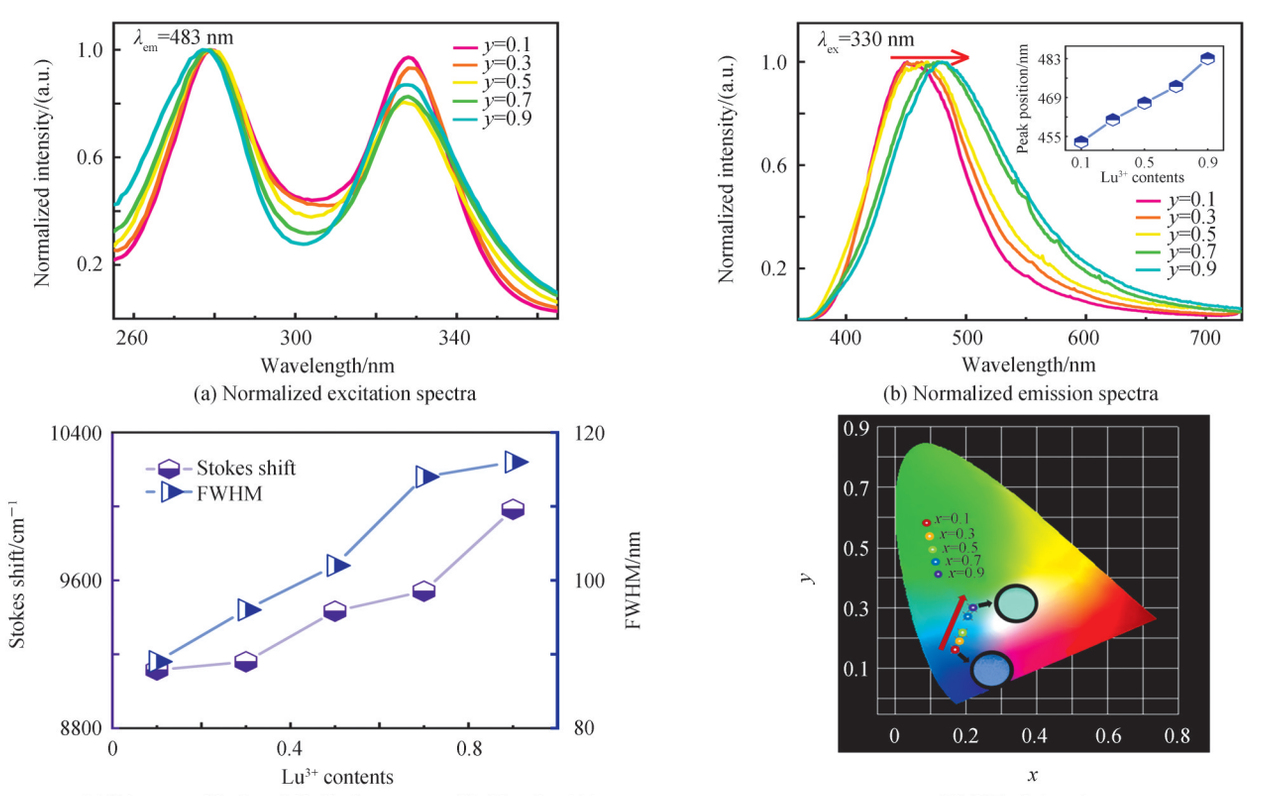

(a) Normalized excitation spectra　　(b) Normalized emission spectra

(c) Diagram of Stokes shift displacement and half peak width　　(d) CIE of phosphors

图6　CGLGO:0.04Bi^{3+}(0.1≤y≤0.9)固溶体荧光粉光谱行为变化

Fig.6　Vary diagram of spectral behavior of CGLGO (0.1≤y≤0.9) solid solution phosphors

Lu^{3+}的引入使晶体场劈裂程度增大、斯托克斯位移增大，导致了光谱发生红移，半峰宽出现展宽。图6(d)是CGLGO:0.04Bi^{3+}(0.1≤y≤0.9)荧光粉在室温下的CIE色度坐标图。图6(d)中能够清晰的观察到CGLGO:0.04Bi^{3+}(0.1≤y≤0.9)荧光粉的发光颜色逐渐由蓝色区域过渡到青色区域，所对应的色坐标由y=0.1时的(0.168 5,0.160 2)移动到y=0.9时的(0.217 9,0.300 7)，而插图是在近紫外光330 nm激发下，蓝色荧光粉和青色荧光粉的照片。

2.5 CGLGO:0.04Bi^{3+}荧光粉的发光热稳定性

热稳定性是评价荧光粉性能的重要因素之一，图7(a)是CGLGO:$x$$Bi^{3+}$($x$=0.04,$y$=0)荧光粉样品的变温光谱。在330 nm激发下，随着温度的升高荧光粉发光强度有所降低。图7(b)为CGLGO:$x$$Bi^{3+}$($x$=0.04,$y$=0)归一化发射峰强度随温度变化图，能够清晰地看到当温度升高到423 K时，荧光粉样品的发光强度保持在初始值的55%，表明该荧光粉热稳定性良好。

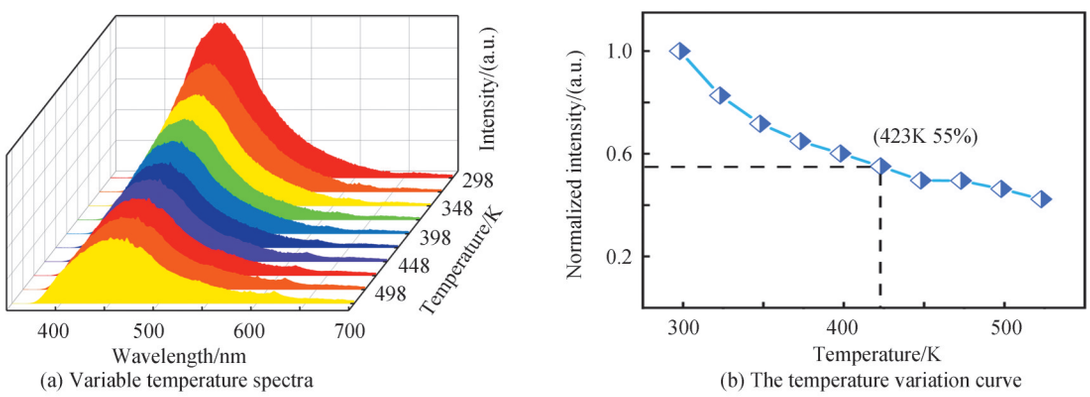

图7 CGLGO:$x$$Bi^{3+}$($x$=0.04,$y$=0)荧光粉变温光谱和变温度曲线

Fig.7 Variable temperature spectra and temperature vary curve of CGLGO:$x$$Bi^{3+}$ (x=0.04, y=0)

3 结论

本文采用高温固相法合成了一系列$Cs_3Gd_{1-x}Ge_3O_9$:$x$$Bi^{3+}$(0.02≤$x$≤0.1)蓝色荧光粉，当$x$=0.04 mol时，$Cs_3Gd_{1-x}Ge_3O_9$:$x$$Bi^{3+}$样品的荧光强度达到最大值；通过等价阳离子替代策略，用Lu^{3+}替代Gd^{3+}获得了一系列发光颜色可调的$Cs_3Gd_{0.96-y}Lu_yGe_3O_9$:0.04$Bi^{3+}$(0.1≤$y$≤0.9)固溶体荧光粉。通过XRD、稳态光谱和荧光寿命测试，证实我们合成了纯相的$Cs_3Gd_{1-x}Ge_3O_9$:$x$$Bi^{3+}$荧光粉，该荧光粉发射主峰位于452 nm，呈现蓝光发射。引入Lu^{3+}离子调控发光中心Bi^{3+}周围的局部微结构，使得荧光粉样品的发射光谱从453 nm蓝色发光红移至483 nm青色发光，半峰宽由88 nm展宽至116 nm，色坐标从蓝色区域(0.168 5,0.160 2)过渡到青色区域(0.217 9,0.300 7)。Lu^{3+}的引入使荧光粉的晶胞和结构发生变化、光谱发生红移，这些光谱行为的变化归因于晶体场劈裂程度增大和斯托克斯位移增大。最后，还探究了x=0.04,y=0时，$Cs_3Gd_{1-x-y}Lu_yGe_3O_9$:$x$$Bi^{3+}$固溶体荧光粉的发光热稳定性，当温度升高到423 K时，发光强度保持在初始值的55%。研究结果表明，本文合成了一系列发光颜色可调的固溶体荧光粉在全光谱照明、植物照明等领域具有潜在的应用价值。

参考文献

[1] ZHANG Weibin, LI Yongwang, YE Shanshan, et al. Full-visible-spectrum lighting realized by a novel Eu^{2+}-doped nitride-based cyan-emitting phosphor[J]. Dalton Transactions, 2021, 50(30): 10446-10454.

[2] SMET P F, PARMENTIER A B, POELMAN D. Selecting conversion phosphors for white light-emitting diodes[J]. Journal of the Electrochemical Society, 2011, 158(6): R37-R54.

[3] LIU Quan, XIONG Puxian, LIU Xiaoqi, et al. Deep red $SrLaGa_3O_7$:Mn^{4+} for near ultraviolet excitation of white light LEDs[J]. Journal of Materials Chemistry C, 2021, 9(11): 3969-3977.

[4] DU Fu, ZHUANG Weidong, LIU Ronghui, et al. Effect of Y^{3+} on the local structure and luminescent properties of $La_{3x}Y_xSi6N_{11}$:Ce^{3+} phosphors for high power LED lighting[J]. RSC Advances, 2016, 6(80): 77059-77065.

[5] LEE S P, HUANG C H, CHAN T S, et al. A new Ce^{3+}-activated thiosilicate phosphor for LED lighting-synthesis, luminescence studies and applications[J]. ACS Applied Materials & Interfaces, 2014, 6(10): 7260-7267.

[6] STROBEL P, BOER T D, WEILER V, et al. Luminescence of an oxonitridoberyllate: a study of narrow-band cyan-emitting $Sr[Be_6ON_4]:Eu^{2+}$[J]. Chemistry of Materials. 2018. 30(9): 3122-3130.

[7] LIU Yongfu, LIU Pu, WANG Lei, et al. Enhanced optical performance by two-step solid-state reactions to synthesize the yellow persistent $Gd_3Al_2Ga_3O_{12}:Ce^{3+}$ phosphor for AC-LED[J]. Chem. Communication. 2017, 53(77): 10636-10639.

[8] FANG Muhuai, NI Chenchen, ZHANG Xuejie, et al. Enhance color rendering index via full spectrum employing the important key of cyan phosphor[J]. ACS Applied Materials & Interfaces, 2016, 8(45): 30677-30682.

[9] ZHOU Yunan, ZHUANG Weidong. Cyan-green phosphor $(Lu_2M)(Al_4Si)O_{12}:Ce^{3+}$ for high-quality LED lamp: tunable photoluminescence properties and enhanced thermal stability.[J]. Inorganic Chemistry, 2019, 58(2): 1492-1500.

[10] CHEN Guantong, LI Yanfeng, MA Xiaole, et al. $YScSi_4N_6C:Ce^{3+}$-a broad cyan-emitting phosphor to weaken the cyan cavity in full-spectrum white light-emitting diodes[J]. Inorganic Chemistry, 2017, 56(18): 11087-11095.

[11] WU Zhanchao, YANG Lina, LIU Jie, et al. Luminescent properties of Eu^{2+} in $BaCdP_2O_7$: Eu^{2+} phosphor: experimental and theoretical analysis[J]. Dyes and Pigments, 2018, 149: 158-166.

[12] TIAN Yue, FENG Ningning, WIECZOREK M W, et al. Energy transfer-induced tunable emission color and thermal quenching of $Ca_3Y(PO_4)_3$: Eu^{2+}, Mn^{2+} phosphor for NUV-pumped white LEDs.[J]. Dyes and Pigments, 2016, 131: 91-99.

[13] KUNIMI S, FUJIHARA S. Elaboration of blue-emitting blue pigments based on Eu^{2+}/Co^{2+} codoped $BaMgAl_{10}O_{17}$ through the heterogeneous distribution of dopants[J]. Dyes and Pigments, 2011, 91(1): 49-54.

[14] JI Changyan, XIAO Shuangyan, HUANG Zhongsheng, et al. High color purity blue emitting phosphors Gd_2 $MgTiO_6$: Bi^{3+} for white light emitting diodes: synthesis and luminescence properties[J]. Chinese Journal of Luminescence, 2020, 41(5): 529-535.
汲长艳，肖双燕，黄中胜，等. 高色纯度白光LED用蓝光材料$Gd_2MgTiO_6:Bi^{3+}$的合成及性能[J]. 发光学报，2020，41(5)：529-535.

[15] KANG Fengwen, YANG Xiaobao, PENG Mingying, et al. Red photoluminescence from Bi^{3+} and the influence of the oxygen-vacancy perturbation in $ScVO_4$: a combined experimental and theoretical study[J]. Journal of Physical Chemistry C, 2014, 118(14): 7515-7522.

[16] WANG Xiu, WANG Jia, LI Xingyu, et al. Novel bismuth activated blue-emitting phosphor $Ba_2Y_5B_5O_{17}:Bi^{3+}$ with strong NUV excitation for WLEDs[J]. Journal of Materials Chemistry C, 2019, 7(36): 11227-11233.

[17] KANG Fengwen, ZHANG Yi, WONDRACZEK L, et al. Processing-dependence and the nature of the blue-shift of Bi^{3+}-related photoemission in $ScVO_4$ at elevated temperatures[J]. Journal of Materials Chemistry C, 2014, 2(46): 9850-9857.

[18] LIANG Dongbao, ZHANG Rui, SHEN Yufang, et al. Synthesis and luminescent properties of $BaLaGa_3O_7$: Bi^{3+} Phosphors[J]. Acta Photonica Sinica, 2022, 51(3):0316002.
梁冬宝，张瑞，申玉芳，等. $BaLaGa_3O_7:Bi^{3+}$荧光粉的制备及发光性能研究[J]. 光子学报，2022，51(3)：0316002.

[19] LIU Dongjie, DANG Peipei, YUN Xiaohua, et al. Luminescence color tuning and energy transfer properties in $(Sr,Ba)_2LaGaO_5$: Bi^{3+}, Eu^{3+} solid solution phosphors: realization of single-phased white emission for WLEDs[J]. Journal of Materials Chemistry C, 2019, 7(43): 13536-13547.

[20] YOUSIF A, SWART H C. Colour tuneable emission from $(Y_{1.995-x}Ga_x)_2O_3$: Bi^{3+} phosphor prepared by a sol-gel combustion method[J]. Materials Letters, 2017, 186: 345-348.

[21] MORRISON G, SPAGNUOLO N R, KARAKALOS S G, et al. $Cs_3RE^{III}Ge_3O_9$ (RE= Pr, Nd, and Sm - Yb) and $Cs_8Tb^{III}_2Tb^{IV}Ge_9O_{27}$: a rare example of a mixed-valent Tb(III)/Tb(IV) oxide[J]. Inorganic Chemistry, 2019, 58(13): 8702-8709.

[22] DANG Peipei, LI Guogang, YUN Xiaohan, et al. Thermally stable and highly efficient red-emitting Eu^{3+}-doped $Cs_3GdGe_3O_9$ phosphors for WLEDs: non-concentration quenching and negative thermal expansion[J]. Light: Science & Applications, 2021, 10(1): 1-13.

[23] TAMBOLI S, NAIR G B, KROON R E, et al. Color tuning of the $Ba_{1.96}Mg(PO_4)_2:0.04Eu^{2+}$ phosphor induced by the chemical unit co-substitution of the $(BO_3)^{3-}$ anion group[J]. Journal of Alloys and Compounds, 2021, 864: 158124-158135.

[24] HAN Jin, PAN Fengjuan, MOLOKEEV M S, et al. Redefinition of crystal structure and Bi^{3+} yellow luminescence with strong near-ultraviolet excitation in $La_3BWO_9:Bi^{3+}$ phosphor for white light-emitting diodes[J]. ACS Applied Materials &

Interfaces, 2018, 10(16): 13660-13668.

[25] LU Jinfeng, MU Zhongfei, ZHU Daoyun, et al. Luminescence properties of Eu^{3+} doped $La_3Ga_5GeO_{14}$ and effect of Bi^{3+} co-doping[J]. Journal of Luminescence, 2018, 196: 50-56.

[26] ZHAO Ming, ZHANG Qinyuan, XIA Zhiguo. Structural engineering of Eu^{2+} -doped silicates phosphors for LED applications[J]. Accounts of Materials Research, 2020, 1(2): 137-145.

[27] LI Wanlu, DAI Pengpeng. Luminescence characteristics of polyaluminate broadband cyan phosphor[J]. Chinese Journal of Luminescence, 2021, 42(9): 1376-1385.
李婉璐,戴鹏鹏. 多铝酸盐宽带青色荧光粉发光特性[J]. 发光学报, 2021, 42(9): 1376-1385.

Preparation and Luminescence Properties of Color-tunable Emission $Cs_3Gd_{1-x-y}Lu_yGe_3O_9:xBi^{3+}$ Solid Solution Phosphor

KANG Xinwei, DAI Pengpeng

(*Xinjiang Key Laboratory for Luminescence Minerals and Optical Functional Materials*, *School of Physics and Electronic Engineering*, *Xinjiang Normal University*, *Urumqi* 830054, *China*)

Abstract: Phosphor-converted White Light-Emitting Diodes (pc-WLEDs) have energy-saving, environmental protection and other excellent performance. At present, the commercial WLEDs are composed of blue LED chip combined with $Y_3Al_5O_{12}:Ce^{3+}$ yellow phosphor. However, due to the lack of red components in the emission spectrum, the white light generated by this method has a low color rendering index (CRI<75) and a high correlation color temperature (CCT>4 500 K), which cannot satisfy the needs of indoor lighting. Researchers at home and abroad have proposed an improved method to generate white light by excitation of red, green and blue phosphors by a near-ultraviolet LED chip. Although this method can produce warm white light for indoor illumination, there is a significant cyan gap in the cyan region of the visible spectrum (480~520 nm), which makes it challenging to achieve full spectral illumination. Therefore, it is desirable to obtain a cyan luminescent material that can achieve full spectrum illumination by mixing phosphors. It is well known that rare-earths Eu^{2+} and Ce^{3+} have been widely used as activator ions in inorganic phosphors. However, Eu^{2+}/Ce^{3+} activated phosphors have spectral overlap in the visible region, resulting in low luminescence efficiency and color drift of the synthesized devices. Compared with rare earth ions, Bi^{3+} hardly absorbs in the visible region, so Bi^{3+} activated phosphors can effectively avoid the spectral reabsorption problem encountered by rare earth Eu^{2+}/Ce^{3+}. At the same time, the outermost electrons 6s and 6p of Bi^{3+} are exposed and sensitive to the changes of crystal field environment, so Bi^{3+} is considered as an activator ion that can realize the color-tunable of phosphors luminescence. Therefore, the abundant optical properties of bismuth ions have attracted extensive attention. In this paper, a series of $Cs_3Gd_{1-x}Ge_3O_9:xBi^{3+}$ ($0.02\leqslant x\leqslant 0.1$) blue phosphors were synthesized by the traditional high-temperature solid-state method. The local environment around Bi^{3+} is regulated by replacing Gd^{3+} in the matrix with Lu^{3+}. A series of $Cs_3Gd_{0.96-y}Lu_yGe_3O_9:0.04Bi^{3+}$ ($0.1\leqslant y\leqslant 0.9$) solid solution phosphors with color-tunable were prepared. The phase structure, luminescence properties, fluorescence lifetime, and thermal stability of the phosphors were characterized by X-ray diffraction, steady-state/transient fluorescence spectra and variable temperature spectra. The results showed that a series of pure phase $Cs_3Gd_{0.96-y}Lu_yGe_3O_9:0.04Bi^{3+}$ compounds were successfully synthesized. Under the excitation of the ultraviolet light wavelength of 330 nm, the emission peak of $Cs_3Gd_{1-x}Ge_3O_9:xBi^{3+}$ phosphor is located at 452 nm, showing blue emission. The broadband emission peak originates from the $^3P_1 \rightarrow {}^1S_0$ transition of Bi^{3+}. When the Bi^{3+} doping concentration is 0.04 mol, the luminescence intensity of $Cs_3Gd_{1-x}Ge_3O_9:xBi^{3+}$ phosphor reaches the maximum value. Under the optimal Bi^{3+} doping concentration, by substituting Lu^{3+} for Gd^{3+}, the emission peak of $Cs_3Gd_{0.96-y}Lu_yGe_3O_9:0.04Bi^{3+}$ gradually redshifted. With the gradual increase of Lu^{3+} doping concentration, the emission peak gradually redshifted from 453 nm at $x=0.1$ mol to 483 nm at $x=0.9$ mol, the corresponding half-peak width is widened from 88 nm to 116 nm, and the color coordinates transition from the blue region (0.168 5, 0.160 2) to the cyan region (0.217 9, 0.300 7). The change of spectral behavior is attributed to the increase of crystal field splitting degree and stokes shift displacement. The luminescence thermal stability of $x=0.04$ mol and $y=$

0.5 mol samples was investigated, and the luminescence intensity of the samples remained 55% of the initial value when the temperature was raised to 423 K. A series of solid solution phosphors with adjustable luminescence color obtained have potential applications in the fields of full spectrum lighting and plant lighting.

Key words: Color-tunable; Solid solution; Bi^{3+} doped; Broadband emission; Full spectrum

OCIS Codes: 160.6990; 160.2540; 160.4670; 160.4760

Foundation item: National Natural Science Foundations of China (No. 51762040), the Project of Outstanding Youths of Xinjiang Ministry of Science and Technology (No. 2021D01E19), Research Fund of Xinjiang Normal University Key Laboratory for Mineral Luminescence and Microstructure (No.KWFG202208)